Evolutionary search for cobalt-rich compounds in the yttrium-cobalt-boron system

Takahiro Ishikawa [1,*] Taro Fukazawa [2,1] Guangzong Xing [1] Terumasa Tadano [3,1] and Takashi Miyake [2,1]

[1] *ESICMM, National Institute for Materials Science, 1-2-1 Sengen, Tsukuba, Ibaraki 305-0047, Japan*

[2] *CD-FMat, National Institute of Advanced Industrial Science and Technology, 1-1-1 Umezono, Tsukuba, Ibaraki 305-8568, Japan*

[3] *CMSM, National Institute for Materials Science, 1-2-1 Sengen, Tsukuba, Ibaraki 305-0047, Japan*

(Received 3 February 2021; accepted 3 May 2021; published 17 May 2021)

Modern high-performance permanent magnets are made from alloys of rare earth and transition metal elements, and large magnetization is achieved in the alloys with a high concentration of transition metals. We applied an evolutionary search scheme based on first-principles calculations to the Y-Co-B system and predicted 37 cobalt-rich compounds with a high probability of being stable. Focusing on remarkably cobalt-rich compounds, YCo_{16} and YCo_{20}, we found that, although they are metastable phases, the phase stability is increased with an increase of temperature due to the contribution of vibrational entropy. The magnetization and Curie temperature are higher by 0.22 T and 204 K in YCo_{16} and by 0.29 T and 204 K in YCo_{20} than those of Y_2Co_{17}, which has been well studied as a strong magnetic compound.

DOI: 10.1103/PhysRevMaterials.5.054408

I. INTRODUCTION

Rare-earth magnets are strong permanent magnets, which mainly consist of rare-earth elements and 3*d* transition metals (Fe and/or Co). High Fe/Co concentration gives rise to high magnetization, and rare earths are a source of high magnetocrystalline anisotropy, which is essential for high coercivity. Rare-earth magnets have been developed since the discovery of large magnetocrystalline anisotropy in an alloy of yttrium and cobalt, YCo_5 [1]. Neodymium magnets are the strongest type of permanent magnet commercially available, and their main phase is formed by the $Nd_2Fe_{14}B$ compound [2], which has a saturation magnetization of 1.85 T at 4.2 K, a magnetocrystalline anisotropy field of 5.3 MA/m at room temperature, and a Curie temperature of 586 K [3].

The magnetization is expected to be further increased using compounds richer in iron than $Nd_2Fe_{14}B$, and RT_{12} (R = rare earth; T = Fe, Co) systems have attracted considerable attention as potential candidates for permanent magnets stronger than $Nd_2Fe_{14}B$ [4–6]. It has long been known that RT_{12} compounds are thermodynamically unstable in bulk form and are stabilized by partial substitution of the third element for T, i.e., $R(T_{1-x}X_x)_{12}$ (X = Al, Si, Ti, V, Cr, Nb, Mo, W) [7–13]. However, the magnetization decreases with the increase of x, and a search is currently underway for the best third elements, in other words, the elements maximizing the stabilization and minimizing the decrease of the magnetization. On the other hand, thin films of $NdFe_{12}N_x$ and $Sm(Fe_{1-x}Co_x)_{12}$ have been fabricated by epitaxial growth on W- and V-buffered MgO(001) substrates. The films have higher magnetization, Curie temperature, and anisotropy field than $Nd_2Fe_{14}B$ [14,15]. In addition, YFe_{12} with the $ThMn_{12}$ structure is experimentally obtained in multiphases by the rapid quenching method [16]. Recently, first-principles calculations predicted that, in YFe_{12} and $Y(Fe_{1-x}Co_x)_{12}$ with x of 0–0.7, the magnetization and Curie temperature are enhanced by the transformation from $ThMn_{12}$ into monoclinic $C2/m$ structures [17].

In the present study, we searched for novel Fe/Co-rich rare-earth compounds using the composition and crystal structure prediction scheme based on first-principles calculations and an evolutionary algorithm. Here, we focus on the Y-Co-B system for the following reasons: (i) Y is favorable for theoretical treatment because it has no f electron in its ground-state electronic configuration, (ii) Co has a hcp structure in the simple substance and is expected to be compatible with Y having hcp compared with Fe having a bcc structure, and (iii) B can play a role in the stabilization of various Y-Co compounds and the formation of novel crystal structures, similar to the case of $Nd_2Fe_{14}B$. As a result, we found 37 cobalt-rich compounds, including remarkably Co rich YCo_{16} and YCo_{20}.

II. COMPUTATIONAL DETAILS

We used the evolutionary construction scheme of a formation-energy convex hull [18] to search for stable compounds in the Y-Co-B system. First, we created an initial set of Y-Co-B compounds using the structure data of analog compounds experimentally reported: YFe_3, Y_6Fe_{23}, Y_3Fe_{29}, $NdFe_2$, $NdFe_5$, Nd_2Fe_{17}, Sm_5Fe_{19}, YB_2, YB_4, CoB, YCo_2B_2, Y_4CoB_{13}, $Nd_2Fe_{14}B$, $Sm_2Fe_{17}N_3$, and $SmCo_3B_2$. They are included in the Materials Project database [19] and the SpringerMaterials database [20]. For simple substances, we used the hcp structures for Co and Y and a rhombohedral $R\bar{3}m$ structure for B. Next, we constructed the preliminary convex hull of the Y-Co-B system by performing the structural optimizations for the compounds in the initial set. Then, by applying evolutionary operators, "mating," "mutation," and "adaptive mutation" [18] to targets selected from compounds

*ISHIKAWA.Takahiro@nims.go.jp

whose distance to the convex hull is small (0–4.4 mRy/atom), compositions and structures with a high probability of being stable were created. Repeatedly performing the creation of compounds and the update of the convex hull, we searched for stable compounds.

We combined our evolutionary construction code with the QUANTUM ESPRESSO (QE) code [21] to perform the optimizations of the structures created by the operators. We used the generalized gradient approximation by Perdew, Burke, and Ernzerhof for the exchange-correlation functional in the framework of the projector augmented wave (PAW) method [22]. We got the PAW potentials from the QE website [23]. The energy cutoff was set at 100 Ry for the wave function and 800 Ry for the charge density. We adopted Marzari-Vanderbilt cold smearing with a width of 0.01 Ry [24]. The maximum number of atoms in the calculation cell is 84, and the k-space integration over the Brillouin zone was carried out on $12 \times 12 \times 12$, $8 \times 8 \times 8$, $6 \times 6 \times 6$, and $4 \times 4 \times 4$ grids for structures including 1–4, 5–12, 13–30, and more than 30 atoms in the calculation cell, respectively. For compounds with a convex-hull distance less than 4.4 mRy/atom, we further increased the k-point grid to achieve a convergence within 0.1 mRy/atom in the total energy.

To investigate the dynamical and thermodynamical stability of the predicted compounds, we calculated phonon dispersion and vibrational free energy using the Vienna Ab initio Simulation Package (VASP) [25] and the PHONOPY code [26]. Second-order interatomic force constants were computed by the finite-displacement method based on harmonic approximation, as implemented in PHONOPY. The total number of atoms in each supercell is ∼100 or larger, which was sufficient to reach the convergence of the vibrational free energy. The energy cutoff for the wave function was set at 400 eV, and the k-point mesh was generated automatically in such a way that the mesh density in the reciprocal space is larger than 450 Å^{-3}. The convergence criteria of energy and force minimization were set to 10^{-8} and 10^{-7} eV, respectively.

For stable compounds, we calculated the intersite magnetic couplings by Liechtenstein's method [27], using AKAIKKR [28], a first-principles program of the Korringa-Kohn-Rostoker (KKR) Green's function method, within the local density approximation. The Curie temperature T_C was evaluated from a classical spin model within the mean-field approximation. Other computational details are the same as the settings in Ref. [29].

III. RESULTS

In this study, we searched for stable and metastable compounds with a convex-hull distance ΔE less than 4.4 mRy/atom (59.8 meV/atom). This tolerance is associated with the approximations and the omission of temperature effects in first-principles calculations [30,31] and the possibility of stabilization by the addition and/or substitution of other elements. We created 4120 structures up to the 11th generation by applying the evolutionary construction technique to the Y-Co-B system ($Y_{1-x-y}Co_xB_y$, $0 \leqslant x \leqslant 1$, $0 \leqslant y \leqslant 1$) and predicted Y_3Co, YCo, YCo_2, YCo_3, Y_6Co_{23}, Y_2Co_{17}, YB_2, YB_3, CoB, YCo_2B_2, YCo_3B_2, and $Y_2Co_{14}B$ as stable

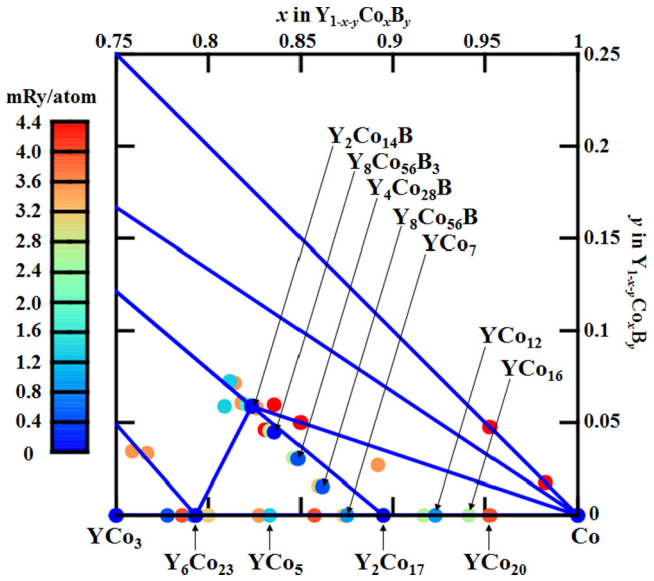

FIG. 1. Projection of the formation-energy convex hull of $Y_{1-x-y}Co_xB_y$ on the xy plane. The solid lines are the edges of the convex hull, and the dots show the compounds with a convex-hull distance less than 4.4 mRy/atom.

compounds on the convex hull (see Fig. S1 in the Supplemental Material (SM) [32]). Figure 1 shows the close-up of the convex hull in the Co-rich region of $0.75 \leqslant x \leqslant 1$, in which we found 4 stable and 33 metastable compounds. The most important observation here is that YCo_{16} and YCo_{20} emerge as compounds richer in Co than YCo_{12}. The ΔE values are 2.72 mRy/atom for YCo_{16} and 3.92 mRy/atom for YCo_{20}. In addition, for the metastable YCo_5 phase, we obtained an orthorhombic *Imma* structure, which is more stable by 0.27 mRy/atom than the $CaCu_5$-type structure used to construct the preliminary convex hull (see Fig. S8 and Table S7 in the SM for the details of the structure [32]). We carefully investigated the energy difference between the two structures by changing the smearing method and obtained 0.27 mRy/atom for Methfessel-Paxton first-order spreading and 0.19 mRy/atom for ordinary Gaussian spreading. Another important point is that $Y_2Co_{14}B$ transforms into YCo_7 with an ordered tetragonal structure $P4_2/mnm$, going through the small energy region of ΔE less than 0.82 mRy/atom. $Y_2Co_{14}B$ takes the $Nd_2Fe_{14}B$-type structure with $P4_2/mnm$ including 4 f.u. in the unit cell. The low-energy path connecting $Y_2Co_{14}B$ and YCo_7 is achieved by a step-by-step elimination of the B atoms from the unit cell (see Fig. S30 in the SM [32]). See Figs. S2–S27 and Tables S1–S26 in the SM for the details of other metastable compounds [32]. Hereafter, we focus on the Co-rich compounds YCo_{16} and YCo_{20}. The structures are assigned as triclinic $P\bar{1}$ for YCo_{16} and monoclinic $C2/m$ for YCo_{20} (see Tables S27 and S28 and Figs. S28 and S29 in the SM for the details of the structures [32]). Figure 2 shows $I4/mmm$ ($ThMn_{12}$-type) YCo_{12} viewed along the b axis, $P\bar{1}$ YCo_{16} viewed along the $[1\bar{1}0]$ direction, and $C2/m$ YCo_{20} viewed along the b axis. $P\bar{1}$ YCo_{16} and $C2/m$ YCo_{20} are achieved by adding the Co atoms to $ThMn_{12}$-type YCo_{12}. YCo_{16} (YCo_{20}) is obtained by the insertion of the four Co atoms per formula unit into the area shown

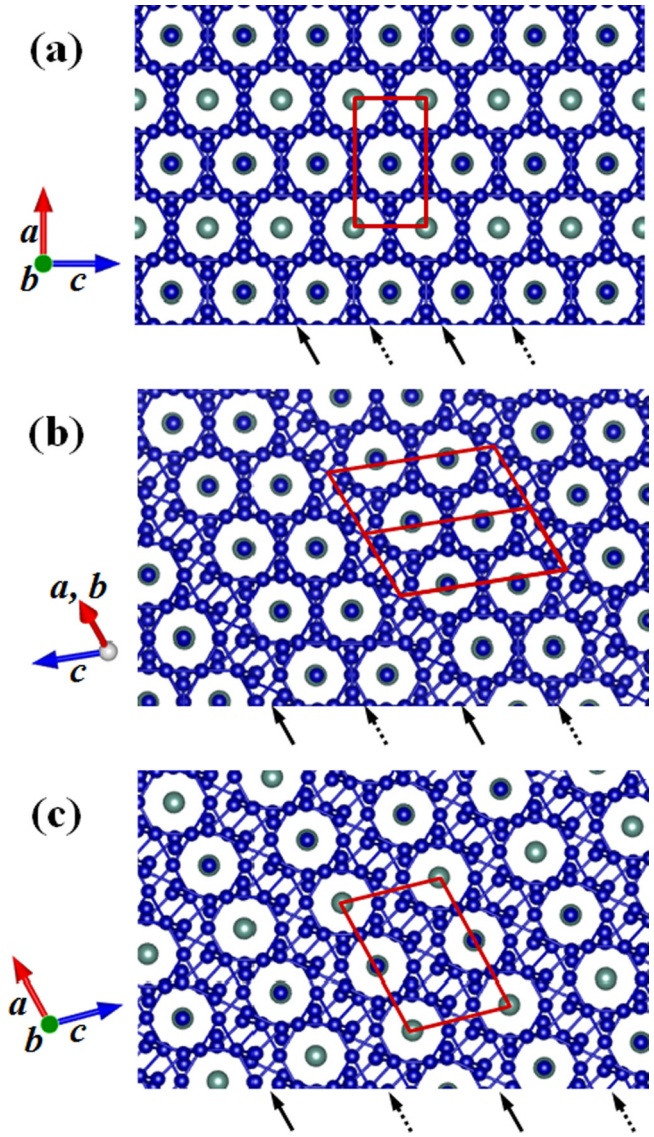

FIG. 2. Crystal structures of (a) YCo_{12} with $I4/mmm$ ($ThMn_{12}$ type) viewed along the b axis, (b) YCo_{16} with $P\bar{1}$ viewed along the $[1\bar{1}0]$ direction, and (c) YCo_{20} with $C2/m$ viewed along the b axis. Frames show the unit cells, and large and small balls represent the Y and Co atoms, respectively. The solid (dashed) arrows show the areas where additional Co atoms are inserted by the transformation from YCo_{12} (YCo_{16}) into YCo_{16} (YCo_{20}). The structures were drawn with VESTA [33].

by the solid (dashed) arrows for YCo_{12} (YCo_{16}), parallel to the (101) plane of $ThMn_{12}$-type YCo_{12}. We investigated the dynamical and thermodynamical stability of YCo_{16} and YCo_{20} by performing phonon calculations. Figure 3 shows the phonon dispersion curves of $P\bar{1}$ YCo_{16} and $C2/m$ YCo_{20}. No imaginary phonon modes were detected in the dispersion curves, which indicates that the two structures are dynamically stable at 0 K. We investigated the variations of the convex-hull distance for YCo_{16} and YCo_{20} with an increase of temperature by considering the entropy contribution, including electronic and vibrational free energies (Fig. 4). We compared the static formation energies of $I4/mmm$ YCo_{12}, $P\bar{1}$ YCo_{16}, and $C2/m$ YCo_{20} between QE and VASP and

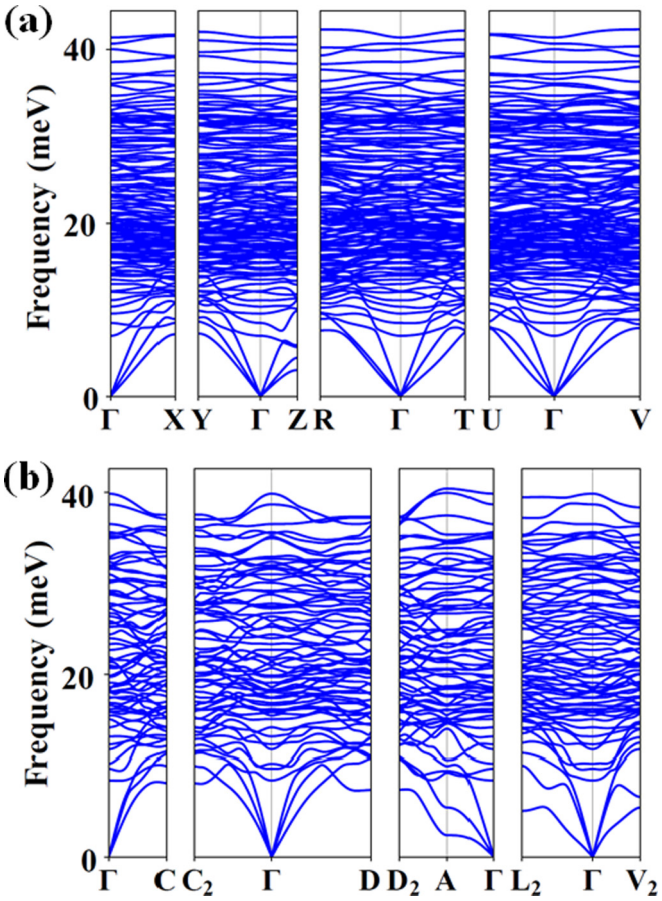

FIG. 3. Phonon dispersions of (a) YCo_{16} with a triclinic P-1 structure and (b) YCo_{20} with a monoclinic $C2/m$ structure.

confirmed the errors are 0.03, 0.12, and 0.32 mRy/atom, respectively. Since these results are reasonably consistent with each other, we discuss the finite-temperature thermodynamic stability of YCo_{16} and YCo_{20} based on the VASP results. The convex-hull distances of YCo_{12}, YCo_{16}, and YCo_{20} almost linearly decrease with the increase of temperature, and the decreasing rate increases as the Co concentration increases:

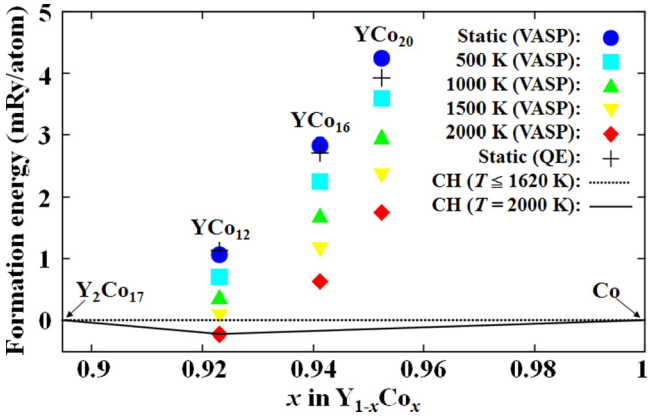

FIG. 4. Phase stability of YCo_{12}, YCo_{16}, and YCo_{20} against the decomposition into Y_2Co_{17} and Co. The dashed and solid lines show the convex hull (CH) at $T \leqslant 1620$ K and $T = 2000$ K, respectively.

TABLE I. Comparison of volume per atom V, magnetic moment per atom m, magnetization M, and Curie temperature T_C for Y_2Co_{17}, YCo_{12}, YCo_{16}, YCo_{20}, Y_2Fe_{17}, YFe_{12}, YFe_{16}, and YFe_{20}.

	Structure	V (Å^3/atom)	m (μ_B/atom)	M (T)	T_C (K)
Y_2Co_{17}	$R\bar{3}m$	12.60	1.354	1.252	1174
				1.25[a]	1167[a]
YCo_{12}	$I4/mmm$	12.15	1.455	1.396	1280
YCo_{16}	$P\bar{1}$	11.90	1.505	1.474	1378
YCo_{20}	$C2/m$	11.77	1.555	1.539	1378
Y_2Fe_{17}	$R\bar{3}m$	13.42	1.979	1.719	720
				1.48[b]	310[c]
YFe_{12}	$I4/mmm$	12.88	2.019	1.826	792
YFe_{16}	$P\bar{1}$	12.65	2.093	1.928	719
YFe_{20}	$C2/m$	12.41	2.053	1.928	434

[a]Experimental data from Ref. [34].
[b]Experimental data from Ref. [35].
[c]Experimental data from Ref. [36].

-0.644 (μRy/atom)/K for YCo_{12}, -1.104 (μRy/atom)/K for YCo_{16}, and -1.247 (μRy/atom)/K for YCo_{20}. With increasing temperature up to 1500 K, the convex-hull distances decrease to 0.07 mRy/atom for YCo_{12}, 1.16 mRy/atom for YCo_{16}, and 2.36 mRy/atom for YCo_{20}. YCo_{12} reaches the convex hull at around 1620 K, and the hull distances of YCo_{16} and YCo_{20} decrease to 0.80 and 1.89 mRy/atom at 2000 K, respectively. Regarding the structure of Y_2Co_{17}, a rhombohedral $R\bar{3}m$ (Th_2Zn_{17}-type) structure is stable in the low-temperature region, while the entropy contributions make the hexagonal $P6_3/mmc$ (Th_2Ni_{17}-type) more stable at temperatures above 780 K. This temperature-induced phase transition was properly considered in the results shown in Fig. 4. Next, we investigated the magnetic properties of $P\bar{1}$ YCo_{16} and $C2/m$ YCo_{20}. Table I lists the volume per atom V, magnetic moment per atom m, total magnetization M, and Curie temperature T_C for Y_2Co_{17}, YCo_{12}, YCo_{16}, and YCo_{20}. The V, m, and M values were calculated by the QE code, and the T_C values were calculated by the AKAIKKR code. See Table S29 in the SM for a comparison of the m values among QE, VASP, and AKAIKKR [32]. The V and m values decrease and increase with the increase of the Co concentration, respectively. Consequently, the M value increases to 1.474 T in YCo_{16} and 1.539 T in YCo_{20}, which are larger than those in Y_2Co_{17} and YCo_{12}. Furthermore, we found that YCo_{16} and YCo_{20} show a T_C value of 1378 K, which is higher by 204 and 98 K than those of Y_2Co_{17} and YCo_{12}, respectively. The T_C value of Y_2Co_{17} is in good agreement with the experimental one, and the trend of the T_C enhancement is realistic.

We also calculated the V, m, M, and T_C values for Fe-based compounds. Although the m value increases with the increase of the Fe concentration from Y_2Fe_{17} through YFe_{16}, it turns to a decrease in YFe_{20} due to the decrease of the magnetic moment of Fe at the 4e site. As a result, the M value increases to 1.928 T in YFe_{16}, whereas there is no further increase in YFe_{20}. In contrast to the case of the Co-based compounds, the T_C value decreases to 719 K in YFe_{16}, which is almost equal to that of Y_2Fe_{17}, and largely decreases in YFe_{20}. The mean-field approximation tends to overestimate T_C, and the calculated T_C value of Y_2Fe_{17} is higher by 410 K than the experimental one. However, it has been reported that the T_C differences among Fe-rich magnetic compounds are satisfactorily reproduced by the mean-field approximation [29,37,38]. Hence, the variations of T_C presented here are realistic, as in the case of the Co-based compounds. We investigated the magnetocrystalline anisotropy of YCo_{16} and YCo_{20}. Figure 5 shows the contour maps of fully relativistic total energies calculated for various spin quantization axes by the VASP code. Here, we treat the energy as a function of the spherical coordinates θ and ϕ, $E(\theta, \phi)$, in which θ is the angle from the axis with the lowest energy (easy axis) toward the high-energy plane perpendicular to it and ϕ is the angle from the axis with the highest energy (hard axis) in the plane. We evaluated the magnetocrystalline

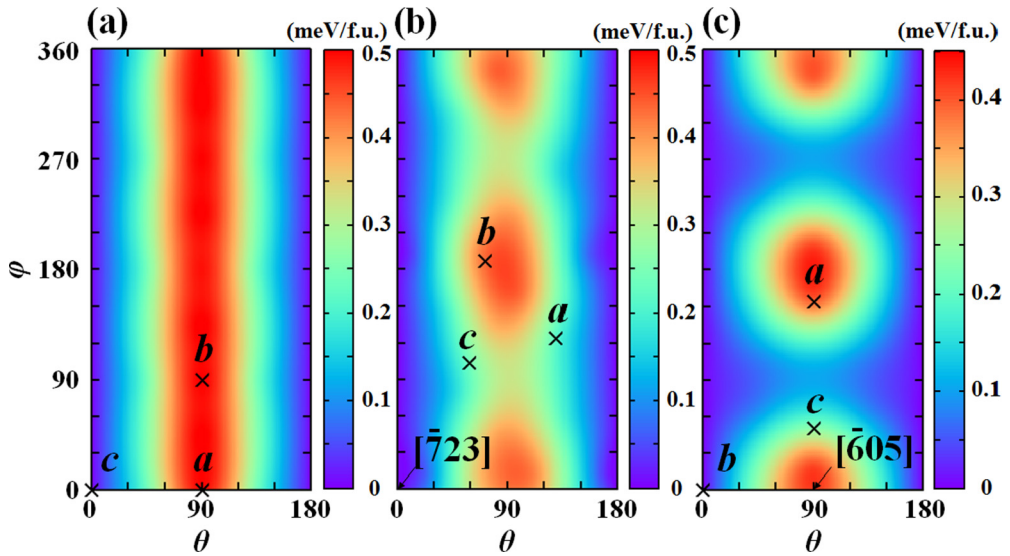

FIG. 5. Contour maps of fully relativistic total energies calculated for various spin quantization axes: (a) $I4/mmm$ YCo_{12}, (b) $P\bar{1}$ YCo_{16}, and (c) $C2/m$ YCo_{20}. The crosses indicate the directions of the crystalline axes of the conventional cells.

anisotropy energy (MAE) as $E(90°, 0) - E(0, 0)$. $I4/mmm$ YCo_{12} has uniaxial anisotropy along the c axis and shows MAE of 0.49 meV/f.u., which is very consistent with the value previously reported [39]. $P\bar{1}$ YCo_{16} has the easy axis along the $[\bar{7}23]$ direction with respect to the conventional cell, whereas the contour map shows a decrease of the uniaxial anisotropy compared with YCo_{12}. MAE is 0.46 meV/f.u., which is comparable to that of YCo_{12}. In contrast to YCo_{12}, $C2/m$ YCo_{20} has in-plane anisotropy with the hard axis along the $[\bar{6}05]$ direction with respect to the conventional cell and shows MAE of 0.44 meV/f.u.

IV. CONCLUSIONS AND DISCUSSION

In conclusion, we searched for stable compounds in the Y-Co-B system, $Y_{1-x-y}Co_xB_y$, using the evolutionary construction technique of a formation-energy convex hull. Focusing on the Co-rich ($0.75 \leqslant x \leqslant 1$) and low-energy ($\Delta E \leqslant$ 4.4 mRy/atom) region, we predicted 34 compounds, including the Co-rich compounds YCo_{16} and YCo_{20}. In addition, we obtained a different stable structure of YCo_5 and a low-energy path connecting $Y_2Co_{14}B$ and YCo_7. Phonon calculations predicted that YCo_{16} and YCo_{20} are dynamically stable and the hull distance ΔH is decreased to 0.80 mRy/atom for YCo_{16} and 1.89 mRy/atom for YCo_{20} with the increase of temperature to 2000 K due to the contribution of the vibrational free energy. The calculated M and T_C values are 1.474 T and 1378 K in YCo_{16} and 1.539 T and 1378 K in YCo_{20}, which are larger than those in Y_2Co_{17} and YCo_{12}. We performed the same calculations for YFe_{16} and YFe_{20} and found that the M values increase, whereas the T_C values decrease.

In this study, we treated the Y-Co-B system, hoping the B atoms play a role in the stabilization of various Y-Co compounds. However, YCo_{16} and YCo_{20} tend to be more unstable when including the B atoms, and further studies are required to clarify how much B contributes to the stabilization of Y-Co compounds. In the Nd-Fe system, B has been known to play an important role in the stabilization of the $Nd_2Fe_{14}B$ compound as follows: $Nd_2Fe_{17} + B \rightarrow Nd_2Fe_{14}B + 3Fe$ [40]. Hence, we expect that new insights into stable phases in R-T-B compounds will be obtained by expanding the present methodology and results to Fe-based systems.

YCo_{16} and YCo_{20} show high magnetization and high Curie temperature, whereas their magnetocrystalline anisotropies decrease compared to that of YCo_{12}, owing to the lowering of the crystalline symmetry from tetragonal to triclinic or monoclinic. Magnetocrystalline anisotropy and coercivity are crucial for the application of RT_{16} and RT_{20} systems to high-performance permanent magnets. Hence, it will be important to accumulate data about their variations by systematically replacing Y with the other R elements and adding third elements and to explore the conditions which cause a further increase of the magnetocrystalline anisotropy.

ACKNOWLEDGMENTS

This work was supported by the Ministry of Education, Culture, Sports, Science and Technology (MEXT) as "The Elements Strategy Initiative Center for Magnetic Materials (ESICMM)" (No. JPMXP0112101004) and the "Program for Promoting Researches on the Supercomputer Fugaku" (DPMSD, Projects No. hp200125 and No. hp210179). The calculations were performed on the Numerical Materials Simulator at NIMS, the ISSP Supercomputer Center at the University of Tokyo, and the supercomputer of ACCMS at Kyoto University.

[1] G. Hoffer and K. Strnat, IEEE Trans. Magn. **2**, 487 (1966).
[2] M. Sagawa, S. Fujimura, H. Yamamoto, and Y. Matsuura, IEEE Trans. Magn. **20**, 1584 (1984).
[3] S. Hirosawa, Y. Matsuura, H. Yamamoto, S. Fujimura, M. Sagawa, and H. Yamauchi, J. Appl. Phys. **59**, 873 (1986).
[4] K. Ohashi, Y. Tawara, R. Osugi, and M. Shimao, J. Appl. Phys. **64**, 5714 (1988).
[5] K. H. J. Buschow, J. Appl. Phys. **63**, 3130 (1988).
[6] Y. Yang, L. Kong, S. Sun, D. Gu, and B. Cheng, J. Appl. Phys. **63**, 3702 (1988).
[7] I. Felner, I. Nowik, and M. Seh, J. Magn. Magn. Mater. **38**, 172 (1983).
[8] K. Ohashi, T. Yokoyama, R. Osugi, and Y. Tawara, IEEE Trans. Magn. **23**, 3101 (1987).
[9] K. Ohashi, Y. Tawara, R. Osugi, J. Sakurai, and Y. Komura, J. Less-Common Met. **139**, L1 (1988).
[10] D. B. D. Mooij and K. H. J. Buschow, J. Less-Common Met. **136**, 207 (1988).
[11] B. Fuquana, J. L. Wang, O. Tegusa, W. Dagula, N. Tang, F. M. Yang, G. H. Wu, E. Brück, F. R. de Boer, and K. H. J. Buschow, J. Magn. Magn. Mater. **290–291**, 1192 (2005).
[12] T. Miyake, K. Terakura, Y. Harashima, H. Kino, and S. Ishibashi, J. Phys. Soc. Jpn. **83**, 043702 (2014).
[13] Y. Harashima, K. Terakura, H. Kino, S. Ishibashi, and T. Miyake, J. Appl. Phys. **120**, 203904 (2016).
[14] Y. Hirayama, Y. K. Takahashi, S. Hirosawa, and K. Hono, Scr. Mater. **95**, 70 (2015).
[15] Y. Hirayama, Y. K. Takahashi, S. Hirosawa, and K. Hono, Scr. Mater. **138**, 62 (2017).
[16] H. Suzuki, AIP Adv. **7**, 056208 (2017).
[17] T. Ishikawa, T. Fukazawa, and T. Miyake, Phys. Rev. Materials **4**, 104408 (2020).
[18] T. Ishikawa and T. Miyake, Phys. Rev. B **101**, 214106 (2020).
[19] A. Jain, S. P. Ong, G. Hautier, W. Chen, W. D. Richards, S. Dacek, S. Cholia, D. Gunter, D. Skinner, G. Ceder, and K. A. Persson, APL Mater. **1**, 011002 (2013).
[20] https://materials.springer.com/.
[21] P. Giannozzi *et al.*, J. Phys.: Condens. Matter **21**, 395502 (2009).
[22] G. Kresse and D. Joubert, Phys. Rev. B **59**, 1758 (1999).
[23] https://www.quantum-espresso.org/pseudopotentials.
[24] N. Marzari, D. Vanderbilt, A. De Vita, and M. C. Payne, Phys. Rev. Lett. **82**, 3296 (1999).
[25] G. Kresse and J. Furthmüller, Phys. Rev. B **54**, 11169 (1996).
[26] A. Togo and I. Tanaka, Scr. Mater. **108**, 1 (2015).

[27] A. I. Liechtenstein, M. I. Katsnelson, V. P. Antropov, and V. A. Gubanov, J. Magn. Magn. Mater. **67**, 65 (1987).
[28] AKAIKKR (m), http://kkr.issp.u-tokyo.ac.jp.
[29] T. Fukazawa, H. Akai, Y. Harashima, and T. Miyake, J. Phys. Soc. Jpn. **87**, 044706 (2018).
[30] Y. Wu, P. Lazic, G. Hautier, K. Persson, and G. Ceder, Energy Environ. Sci. **6**, 157 (2013).
[31] Y. Hinuma, T. Hatakeyama, Y. Kumagai, L. A. Burton, H. Sato, Y. Muraba, S. Iimura, H. Hiramatsu, I. Tanaka, H. Hosono, and F. Oba, Nat. Commun. **7**, 11962 (2016).
[32] See Supplemental Material at http://link.aps.org/supplemental/10.1103/PhysRevMaterials.5.054408 for the formation energy convex hull, stable compounds, and their structure parameters.
[33] K. Momma and F. Izumi, J. Appl. Crystallogr. **44**, 1272 (2011).
[34] K. J. Strnat, *Ferromagnetic Materials* (North-Holland, Amsterdam, 1988), p. 131.
[35] K. Koyama, T. Kajitani, Y. Morii, H. Fujii, and M. Akayama, Phys. Rev. B **55**, 11414 (1997).
[36] Z. Arnold, J. Kamarad, P. A. Algarabel, B. Garcia-Landa, and M. R. Ibarra, IEEE Trans. Magn. **30**, 619 (1994).
[37] T. Fukazawa, H. Akai, Y. Harashima, and T. Miyake, J. Appl. Phys. **122**, 053901 (2017).
[38] T. Fukazawa, H. Akai, Y. Harashima, and T. Miyake, IEEE Trans. Magn. **55**, 2101305 (2019).
[39] L. Ke and D. D. Johnson, Phys. Rev. B **94**, 024423 (2016).
[40] Y. Tatetsu, Y. Harashima, T. Miyake, and Y. Gohda, Phys. Rev. Materials **2**, 074410 (2018).